New perspectives for Rashba spin–orbit coupling

A. Manchon[1]*, H. C. Koo[2,3], J. Nitta[4], S. M. Frolov[5] and R. A. Duine[6]

In 1984, Bychkov and Rashba introduced a simple form of spin–orbit coupling to explain the peculiarities of electron spin resonance in two-dimensional semiconductors. Over the past 30 years, Rashba spin–orbit coupling has inspired a vast number of predictions, discoveries and innovative concepts far beyond semiconductors. The past decade has been particularly creative, with the realizations of manipulating spin orientation by moving electrons in space, controlling electron trajectories using spin as a steering wheel, and the discovery of new topological classes of materials. This progress has reinvigorated the interest of physicists and materials scientists in the development of inversion asymmetric structures, ranging from layered graphene-like materials to cold atoms. This Review discusses relevant recent and ongoing realizations of Rashba physics in condensed matter.

In crystals that lack an inversion centre, electronic energy bands are split by spin–orbit (SO) coupling. More specifically, in non-centrosymmetric zinc-blende or wurtzite semiconductors, bulk SO coupling becomes odd in the electron's momentum p, as originally realized by Dresselhaus[1] and Rashba[2]. After the establishment of modulation-doped semiconductor heterostructures, Vas'ko[3], and Bychkov and Rashba[4] applied this idea to two-dimensional electron gases with structural inversion asymmetry. Odd-in-p SO coupling has been confirmed across a wide variety of materials that lack spatial inversion (Box 1). The essential feature of any SO coupling is that, even in the absence of an externally applied magnetic field, electrons moving in an electric field experience a magnetic field in their frame of motion — the SO field — that couples to the electron's magnetic moment. In the case of a system with inversion symmetry breaking, the odd-in-p SO field enables a wide variety of fascinating phenomena (Box 2). By extension, in this Review we refer to this odd-in-p SO coupling as Rashba SO coupling. The exploration of Rashba physics is now at the heart of the growing research field of spin–orbitronics, a branch of spintronics[5,6] that focuses on the manipulation of non-equilibrium material properties using SO coupling (Fig. 1). Here we review the most recent developments that involve such (odd-in-p) Rashba SO interactions across various fields of physics and materials science.

Spin generation, manipulation and detection

Charge carriers in materials with Rashba SO coupling experience a momentum-dependent effective magnetic field, a spin-dependent velocity correction and a geometric phase resulting from the SO coupling (Box 2). These features are particularly attractive for the realization of device concepts[5,7] in which spin polarization is generated from charge current, manipulated by electric fields and detected as voltage or optical Kerr rotation.

Spin Hall effect. The spin Hall effect is the conversion of an unpolarized charge current into a chargeless pure spin current (that is, a net spin flow without charge flow), transverse to it. This occurs through two types of mechanism. In the first, electrons with different spin projections diffuse towards opposite directions after scattering against SO-coupled impurities. This spin-dependent extrinsic

Mott scattering is at the core of the original prediction of the spin Hall effect formulated 40 years ago by Dyakonov and Perel[8] (and revived recently[9]). The second type of mechanism concerns the spin-dependent distortion of electron trajectories in the presence of a SO-coupled band structure, which gives rise to the intrinsic spin Hall effect[10,11] (Box 2). In ref. 11, researchers predicted the existence of a universal spin Hall conductivity $\sigma_H = e\Phi_B/8\pi^2$ for a ballistic two-dimensional electron gas with Rashba interaction, where Φ_B is the geometrical phase (also called the Berry phase), which is acquired by a state when transported around a loop in momentum space[12].

Experimental observation of the spin Hall effect in bulk GaAs and strained InGaAs was achieved using Kerr rotation microscopy[13]. Without applying any external magnetic fields, an out-of-plane spin polarization with opposite sign on opposite edges of the sample was detected. The amplitude of the spin polarization was weak, and the mechanism was attributed to the extrinsic spin Hall effect. The spin Hall effect was also observed in light-emitting diodes based on a GaAs 2D hole system[14]. In this experiment, the magnitude of the spin polarization was in agreement with that predicted by the intrinsic spin Hall effect. Spin transistors and spin Hall effects have been combined by realizing an all-semiconductor spin Hall effect transistor[15]. A spin AND logic function was demonstrated in a semiconductor channel with two gates. Here, spin-polarized carriers were detected by the inverse spin Hall effect and the spin generation in this device was achieved optically. The search for a large spin Hall effect has been extended to metals[16] and is now one of the most active areas of spintronics. Because these SO effects do not necessitate the breaking of inversion symmetry and are hence not directly related to Rashba physics, we refer the reader to excellent reviews available on this topic[7,17,18].

Spin interference. As mentioned above, spin-polarized electrons that experience Rashba SO coupling acquire a geometrical (Berry) phase that may result in spin interference[12] (Box 2). Indeed, the rotation operator for spin-1/2 produces a minus sign under a 2π rotation. Neutron spin interference experiments have verified this extraordinary prediction of quantum mechanics[19]. A local magnetic field causes precession of the electron's spin in a way that depends on the path of the electron. Spin interference effects controlled by

[1]King Abdullah University of Science and Technology (KAUST), Physical Science and Engineering Division, Thuwal 23955-6900, Saudi Arabia. [2]Center for Spintronics, Korea Institute of Science and Technology (KIST), 39-1 Hawolgok-dong, Seongbukgu, Seoul 136-791, Korea. [3]KU-KIST Graduate School of Converging Science and Technology, Korea University, Seoul 136-701, Korea. [4]Department of Materials Science, Tohoku University, 980-8579 Sendai, Miyagi, Japan. [5]Department of Physics and Astronomy, University of Pittsburgh, Pittsburgh, Pennsylvania 15260, USA. [6]Institute for Theoretical Physics and Center for Extreme Matter and Emergent Phenomena, Utrecht University, Leuvenlaan 4, 3584 CE Utrecht, The Netherlands. *e-mail: aurelien.manchon@kaust.edu.sa

Box 1 | Rashba spin–orbit interaction.

Origin of spin–orbit coupling. When an electron with momentum **p** moves in a magnetic field **B**, it experiences a Lorentz force in the direction perpendicular to its motion $\mathbf{F} = -e\mathbf{p} \times \mathbf{B}/m$ and possesses Zeeman energy $\mu_B\boldsymbol{\sigma} \cdot \mathbf{B}$, where $\boldsymbol{\sigma}$ is the vector of the Pauli spin matrices, m and e are the mass and charge of the electron, respectively, and $\mu_B = 9.27 \times 10^{-24}$ J T^{-1} is the Bohr magneton. By analogy, when this electron moves in an electric field **E**, it experiences a magnetic field $\mathbf{B}_{eff} \sim \mathbf{E} \times \mathbf{p}/mc^2$ in its rest-frame (where c is the speed of light) — a field that also induces a momentum-dependent Zeeman energy called the SO coupling, $\hat{H}_{SO} \sim \mu_B (\mathbf{E} \times \mathbf{p}) \cdot \boldsymbol{\sigma}/mc^2$. In crystals, the electric field is given by the gradient of the crystal potential $\mathbf{E} = -\nabla V$, which produces a SO field $\mathbf{w}(\mathbf{p}) = -\mu_B(\nabla V \times \mathbf{p})/mc^2$. Because SO coupling preserves time-reversal symmetry ($\mathbf{w}(\mathbf{p}) \cdot \boldsymbol{\sigma} = -\mathbf{w}(-\mathbf{p}) \cdot \boldsymbol{\sigma}$), the SO field must be odd in electron momentum **p**; that is, $\mathbf{w}(-\mathbf{p}) = -\mathbf{w}(\mathbf{p})$. This odd-in-$p$ SO field only survives in systems that lack spatial inversion symmetry.

Dresselhaus and Rashba spin–orbit coupling. Dresselhaus[1] was the first to notice that in zinc-blende III–V semiconductor compounds lacking a centre of inversion, such as GaAs or InSb, the SO coupling close to the Γ point adopts the form

$$\hat{H}_{D_3} = (\gamma/\hbar)\,((p_y^2 - p_z^2)p_x\sigma_x + \text{c.p.}) \qquad (1)$$

where c.p. denotes circular permutations of indices. Of course, additional symmetry considerations in the band structure result in additional odd-in-p SO coupling terms (see for example, ref. 136). In the presence of strain along the (001) direction, the cubic Dresselhaus SO coupling given in equation 1 reduces to the linear Dresselhaus SO coupling[137]

$$\hat{H}_{D_1} = (\beta/\hbar)\,(p_x\sigma_x - p_y\sigma_y) \qquad (2)$$

where $\beta = \gamma p_z^2$. In quantum wells with structural inversion symmetry broken along the growth direction and respecting the C_{2v} symmetry, Vas'ko[3] and Bychkov and Rashba[4] proposed that the interfacial electric field $\mathbf{E} = E_z\mathbf{z}$ results in a SO coupling of the form

$$\hat{H}_R = (\alpha_R/\hbar)\,(\mathbf{z} \times \mathbf{p}) \cdot \boldsymbol{\sigma} \qquad (3)$$

where α_R is known as the Rashba parameter. In other words, in the solid state the Dirac gap $mc^2 \approx 0.5$ MeV is replaced by the energy gap ~1 eV between electrons and holes, and $\alpha_R/\hbar \gg \mu_B E_z/mc$. This convenient form, derived for 2D plane waves, is only phenomenological and must be applied with precaution to realistic systems. Indeed, theoretical investigations showed that the lack of inversion symmetry does not only create an additional electric field E_z, but also distorts the electron wavefunction close to the nuclei, where the plane-wave approximation is not valid[138]. Therefore, for the discussion provided in this Review, one must keep in mind that the p-linear Rashba SO coupling is a useful approximation that does not entirely reflect the actual form of the SO coupling in inversion-asymmetric systems.

Both Dresselhaus and Rashba SO coupling lock spin to the linear momentum and split the spin sub-bands in energy (Fig. 2a). Such band splitting is also observed at certain metallic surfaces (Fig. 2b). The illustration below shows the spin texture at the Fermi surface in the case of Rashba (panel **a**) and strain-induced (panel **b**) p-linear Dresselhaus SO coupling. In the example shown in panel **c**, when both are present with equal magnitude, the SO field aligns along the [110] direction, resulting in, for instance, the suppression of spin relaxation interaction in this direction[43].

Measuring Rashba spin–orbit coupling. The magnitude of the phenomenological Rashba parameter α_R has been estimated for a wide range of materials that present either interfacial or bulk inversion symmetry breaking. The analysis of Shubnikov-de Haas oscillations and spin precession in InAlAs/InGaAs[23,139] (Fig. 2c) yields a Rashba parameter (~0.67 × 10^{-11} eV m) comparable to recent estimations at the surface of SrTiO$_3$(001) single crystals using weak localization measurements[140] (~0.5 × 10^{-11} eV m). Signatures of Rashba SO coupling have also been confirmed at the surface of heavy metals such as Au (ref. 141), Ir (ref. 142) or √3 × √3 BiAg(111) alloys[135], using ARPES, and revealing a Rashba effect that is two orders of magnitude larger than in semiconductors (~3.7 × 10^{-10} eV m for BiAg(111) alloy). More recently, topological insulators have been shown to display comparable Rashba parameters (~4 × 10^{-10} eV m for Bi$_2$Se$_3$; ref. 143). Structures that present bulk inversion symmetry breaking also show evidence of a Rashba-type SO splitting of the band structure. For instance, the polar semiconductor BiTeI displays a bulk Rashba parameter[144] (~3.85 × 10^{-10} eV m) as large as that found on the surface of topological insulators. Finally, large SO coupling at Fe/GaAs (ref. 145) and IrMn/MgO (ref. 146) interfaces has been reported, resulting in a change of tunnelling resistance as a function of the magnetization direction, known as tunnelling anisotropic magnetoresistance.
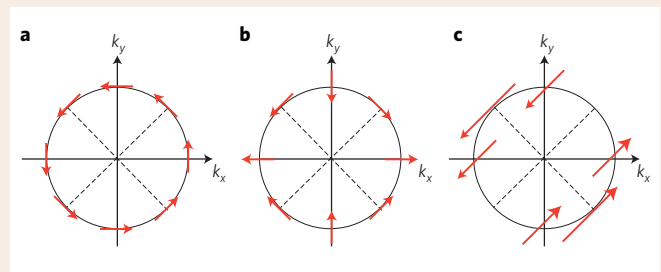
Spin texture at the Fermi surface. a,b, Spin texture due to Rashba (**a**) and linear (**b**) Dresselhaus SO coupling when strain is applied along [001]. **c,** When both are present with equal magnitude, the SO field aligns along [110]. The arrows represent the SO field.

an electric field — distinct from conventional spin interference — have been demonstrated in a single HgTe ring[20] and in small arrays of mesoscopic InGaAs two-dimensional electron gas rings[21] with strong Rashba SO coupling. This interference is an Aharonov–Casher[22] effect and is the electric analogue of the Aharonov–Bohm effect, which governs the interference of propagating electronic waves in the presence of a magnetic field. The spin precession rate can be controlled in a precise and predictable way with an electrostatic gate[23].

Spin galvanic effect. Locking between the electron momentum and its spin results in the spin galvanic effect (Box 2). Following the Rashba Hamiltonian (equation 3 in Box 1), the spin galvanic effect is given by $\mathbf{j}_c = -e\alpha_R(\mathbf{z} \times \mathbf{S})/\hbar$, where **S** is the non-equilibrium spin density (created either electrically or optically) and $\mathbf{j}_c$ is the induced charge current density[24]. This concept was originally developed in the context of optical spin manipulation in semiconductors, and was first observed in quantum wells[25,26]. The spin galvanic effect was also recently realized in a NiFe/Ag/BiAg lateral device[27]. In this

Box 2 | Physics of the Rashba effect.

To discuss the physics induced by SO coupling in systems lacking inversion symmetry, let us consider the p-linear Rashba SO coupling introduced previously. Equation 3 in Box 1 describes a Zeeman term that involves a magnetic field proportional to the electron momentum p. Consequently, when electrons flow along the x axis, they experience an effective magnetic field along the y axis, B_{Ry}, called the Rashba field, as depicted in the figure (top). The magnitude of the Rashba field can be calculated from $B_{Ry} = 2\alpha_R k_F/g\mu_B$, where k_F and g are the Fermi wavevector and g-factor of the carriers in the conduction channel, respectively.

Rashba field and spin precession. When the electron spin is not aligned with the Rashba field, spin precession takes place with a frequency that depends on the magnitude of the field. In the bottom panel, the spin-polarized electrons injected along the x axis precess under the influence of the Rashba field, even without an applied magnetic field. The magnitude of the electric field, and hence the strength of the Rashba field and spin precession rate, can be controlled by a gate voltage[23,31–33] (Fig. 2c). In the diffusive regime, this precession is at the origin of the Dyakonov–Perel spin-relaxation mechanism[42]. An interesting consequence of the emergence of the Rashba field is the possibility to polarize flowing electrons along the direction of this field. This is known as the inverse spin galvanic effect[28]. This effect has a counterpart referred to as the spin galvanic effect[25], in which non-equilibrium spin density (created by either optical or electrical means) is converted into a charge current.

Berry curvature and spin Hall effect. The Rashba effect modifies the velocity according to $\mathbf{v}_a = \partial_{\mathbf{p}}\hat{H}_R = -(\alpha_R/\hbar)\mathbf{z} \times \boldsymbol{\sigma}$. Physically, SO coupling 'bends' the trajectory of the electrons in a manner very similar to how Magnus force distorts the trajectory of spinning balls in classical mechanics. The direction of the distortion depends on the direction of the angular momentum (that is, of the spinning), which results in the spin Hall effect (Fig. 1). This additional velocity can be formulated in terms of an effective Lorentz force acting on the electron semiclassical wavepacket. The effective magnetic field that produces this Lorentz force is called the Berry curvature[12], $\boldsymbol{\Omega}(\mathbf{p}) \propto \alpha_R\nabla_{\mathbf{p}} \times (\boldsymbol{\sigma} \times \mathbf{p})$, which depends only on the geometry of the band structure. The resulting anomalous velocity induces an off-diagonal conductivity that can be non-zero if time-reversal symmetry is broken. The language of Berry curvature and its associated Berry phase has been extremely successful in describing the various properties of Rashba and Dirac materials[12].
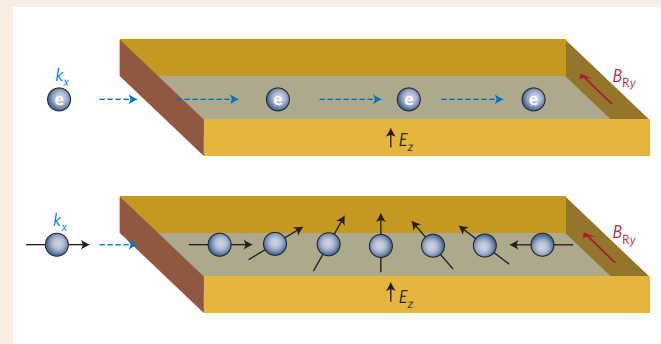
Inverse spin galvanic effect and spin precession. Top: Moving electrons (k_x) with a perpendicular electric field (E_z) experience the Rashba field, B_{Ry}. Bottom: In a Rashba system, the spin of the moving electrons (arrows) precesses around the axis of the Rashba field.

---

system, a spin current is pumped from NiFe into Ag, where it is converted into a transverse charge current through the spin galvanic effect, which takes place at the Ag/BiAg interface. The inverse spin galvanic effect — the Onsager reciprocal of the spin galvanic effect (sometimes called the Edelstein effect[28]) — has recently been observed in strained semiconductors[29] and quantum wells[30]. Following from the Rashba symmetry, the spin density generated by the current is $\mathbf{S} = \alpha_R m(\mathbf{z} \times \mathbf{j}_c)/e\hbar$. This is of particular significance when electrically manipulating the magnetization of ferromagnets (see below).

Electrical spin manipulation. An essential aspect that renders Rashba SO coupling particularly attractive for spintronics and quantum computation is its ability to be controlled by an external gate voltage across a heterojunction containing a two-dimensional electron gas. Indeed, because the strength of the Rashba parameter is directly related to the interfacial potential drop (Box 1), applying a gate voltage modifies the quantum well asymmetry and electron occupation, which in turn controls the magnitude of the Rashba SO coupling, as experimentally demonstrated in InGaAs/InAlAs heterostructures[23] and HgTe quantum wells[31] (Fig. 2c,d). The electric control of spin states is superior to magnetic field control owing to its better scalability, lower power consumption and the possibility for local manipulation of spin states. The first spintronic device concept that utilized Rashba SO coupling was a spin field-effect transistor[32]. The implementation of this transistor relied on spin injection from a ferromagnetic electrode into a two-dimensional electron gas and, subsequently, on gate-controlled precession angle of the injected electron's spin. Spin injection was then combined with precession towards the spin field-effect transistor[33].

A Stern–Gerlach spin filter was proposed by using the spatial gradient of the Rashba interaction[34]. In the traditional Stern–Gerlach experiment, particles that possess opposite magnetic moment are deflected towards opposite directions by a gradient in the magnetic field. In ref. 34, a spatial gradient of the effective magnetic field due to the Rashba SO coupling is shown to cause a spin separation. Almost 100% spin polarization can be realized, even without applying any external magnetic fields or using ferromagnetic contacts. In contrast with the spin Hall effect, the spin-polarized orientation is in-plane. This inhomogeneous SO-induced electronic spin separation has been demonstrated in semiconductor quantum point contacts[35]. Such a spin-filter device can be used for electrical spin detection[36].

Electron spin resonance involves using static and oscillating magnetic fields to manipulate individual electron spins for quantum information processing. The oscillating field induced by Rashba and Dresselhaus SO coupling and driven by the ballistic bouncing motion of electrons was used to induce spin resonance without external a.c. fields[37]. Coherent control of individual electron spins using gigahertz electric fields by means of electric dipole spin resonance has been performed in GaAs/AlGaAs gate-defined quantum dots[38] and in InAs nanowires[39], thereby establishing SO qubits. Rabi frequencies exceeding 100 MHz were demonstrated in InSb nanowires[40]. The demonstration of SO qubits coupled to superconducting resonators paves the way for a scalable quantum computing architecture[41].

Suppressing spin relaxation. In the above discussion, we have highlighted the efficient coupling of the electron's spin to its motion, and the ways in which this can be used to control spin. Unfortunately, the momentum-changing scattering of an electron moving through
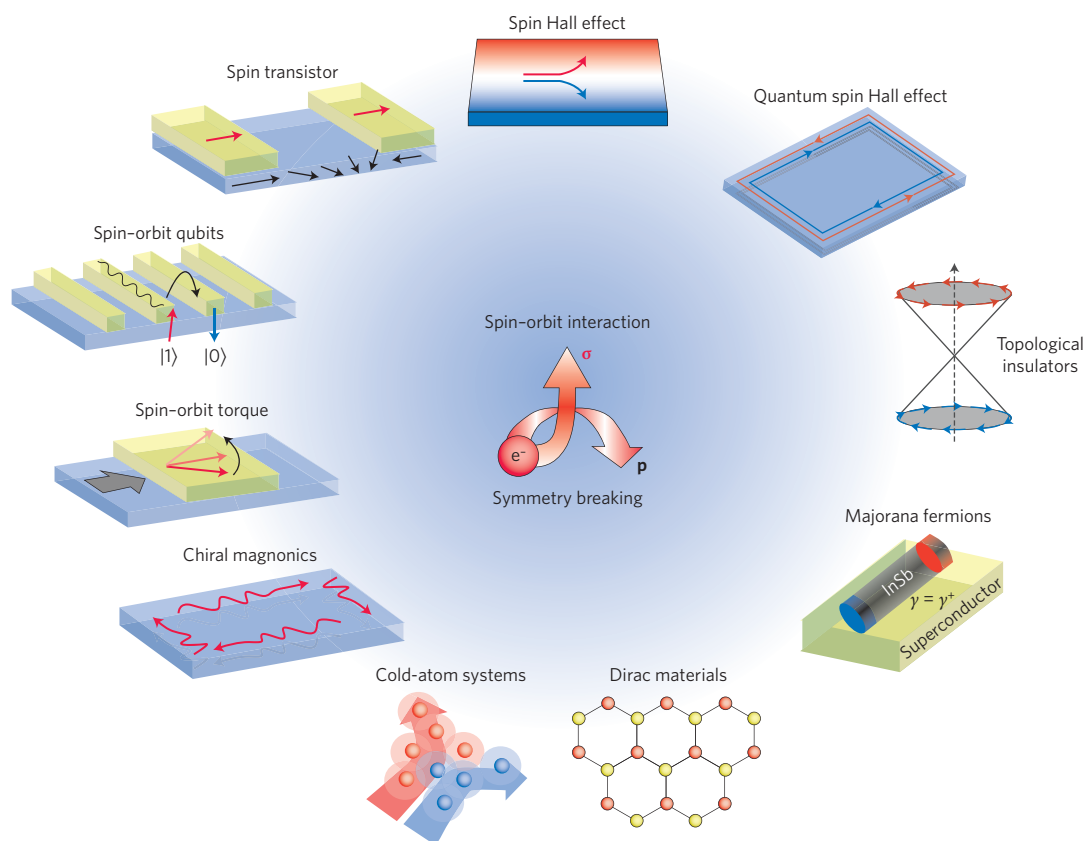
Figure 1 | Various realizations of spin–orbitronics. When SO coupling is present in systems with broken inversion symmetry, unique transport properties emerge that give birth to the tremendously active field of spin–orbitronics, which is the art of manipulating spin using SO coupling. This figure illustrates the various sub-fields in which magnetization and spin directions (denoted by red and blue arrows, respectively) can be manipulated electrically, and where novel states of matter have been revealed.

a semiconductor causes sudden changes in the effective SO magnetic field, which leads to spin randomization[42]. Suppressing spin relaxation in the presence of strong, tunable SO coupling is therefore a major challenge in semiconductor spintronics[5]. Such suppression is possible in group III–V semiconductor heterostructures when both linear Dresselhaus and interfacial Rashba SO coupling are present. In the special case where both SO interactions are equal in magnitude ($\alpha_R = \beta$), the total SO field aligns along [110] (or [–110] when $\alpha_R = -\beta$), which quenches spin relaxation in this direction[43] (Box 1). This spin conservation is predicted to be robust against all forms of spin-independent scattering, including electron–electron interactions, but is broken by spin-dependent scattering and p-cubic Dresselhaus terms[44].

Under this condition ($|\alpha_R| = |\beta|$), a persistent spin helix (that is, a spin spiral extending along the (110) directions) can be stabilized[44,45]. The persistent spin helix in semiconductor quantum wells was confirmed by optical transient spin-grating spectroscopy[46]. The researchers found that the lifetime of the helical texture is enhanced by two orders of magnitude near the exact persistent spin helix point. Recently, gate-controlled spin helix states have been realized using a direct determination of the Rashba and Dresselhaus interactions ratio[47], and spin transistor design based on gate-tunable spin helix has been proposed[44].

Spin–orbit torques in ferromagnets

Electrical control over the magnetization direction of small magnets is currently among the most active areas in spintronics, due to its interest for memory, logic and data-storage applications[5,6]. For the past 15 years, this control has been achieved by transferring spin angular momentum between a flowing spin current and the local

magnetization of a ferromagnet[48,49], as now conventionally observed in magnetic spin-valve structures and magnetic domain walls. Less than 10 years ago, an alternative mechanism based on the inverse spin galvanic effect was proposed, whereby SO coupling mediates direct transfer of the carrier momentum to the local magnetization.

Indeed, in non-centrosymmetric (for example, wurtzite) magnetic semiconductors or asymmetrically grown ultrathin magnetic layers (for example, a ferromagnet deposited on a heavy metal), the spin density generated by the inverse spin galvanic effect exerts a torque on the magnetization[50,51]. This 'SO torque' can be used to excite or reverse the magnetization direction and is therefore potentially useful for applications such as magnetic memories or logic[52]. This torque was first observed in (Ga,Mn)As (ref. 53), where straining the zinc-blende structure is responsible for the emergence of p-linear Dresselhaus SO coupling (Box 1). A year later, SO torques were reported in Pt/Co/AlO$_x$ asymmetric structures and attributed to interfacial Rashba SO coupling[54]. Since then, a number of experimental investigations have revealed the complex nature of the SO torque in magnetic semiconductors[55] and metallic multilayers[56]. A major difficulty is clearly identifying the physical origin of the SO torque, as the spin Hall effect plays an important role in magnetic multilayers[57]. Going beyond the inverse spin galvanic effect paradigm, several mechanisms have been proposed to explain the experimental results, including the emergence of an intrinsic (Berry phase-induced) SO torque[55].

Very large SO torques have also been found at interfaces with topological insulators[58,59], where the Dirac cone expected to emerge at the surface of these materials (see below) is probably dramatically altered by the presence of the ferromagnet. Antiferromagnets might also benefit from the emergence of SO torques. It has recently
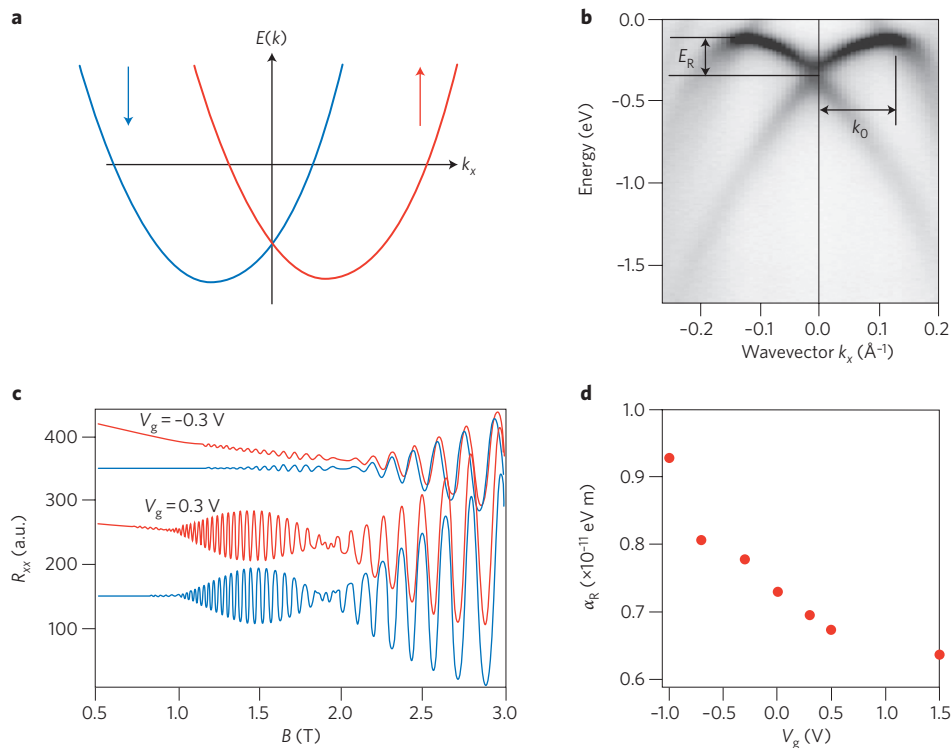
Figure 2 | Rashba spin splitting at interfaces. a, Schematic of the energy dispersion of a 1D free-electron gas with spin–momentum locking induced by Rashba spin–orbit coupling: the two bands carry opposite spin momenta, represented by the red and blue arrows. **b**, Energy dispersion at the surface of a BiAg(111) alloy measured by ARPES[135], with energy shift E_R and momentum offset k_0 being a clear indicator of Rashba splitting. **c**, Shubnikov–de Haas oscillations in an InAlAs/InGaAs quantum well[23], from which the Rashba parameter can be extracted. The longitudinal resistance R_{xx} is represented as a function of the external magnetic field B and for different gate voltages V_g. Red lines are experimental data and blue lines are simulations. **d**, Gate control of the magnitude of the Rashba spin–orbit coupling parameter α_R extracted from the Shubnikov–de Haas oscillations displayed in **c**. Figure reproduced with permission from: **b**, ref. 135, APS; **c,d**, ref. 23, APS.

been theoretically and experimentally demonstrated that SO torque could be utilized to manipulate coherently the order parameter of these materials, which would give promising perspectives for the field of antiferromagnetic spintronics[60,61].

Finally, it is worth mentioning that interfacial or bulk inversion symmetry breaking also has a dramatic impact on the transport properties of spin waves, resulting in coupling effects that are very similar to those experienced by electrons undergoing Rashba SO coupling. In such materials, the magnetic energy acquires an antisymmetric exchange interaction known as the Dzyaloshinskii–Moriya interaction[62,63]. This acts like a Rashba SO coupling on spin waves: the resulting distorted magnetization causes chiral magnetism and possibly generates skyrmions[64], but even more importantly for this Review, the magnon energy dispersion acquires a component that is linear in the magnon momentum, as observed experimentally[65]. This linear component in the dispersion relation induces an anomalous velocity, which leads to the magnon Hall effect[66], orbital moment and edge currents[67]. It was recently proposed that this antisymmetric exchange interaction enables a 'magnon-driven torque' that displays striking similarities to the electron-driven SO torque discussed above[68].

Topological states and Majorana fermions
Spin–orbit interactions play a central role as a design element of the topological states of matter. Here we summarize the topological insulator and topological superconductor states (both remarkable for their edge states), which are characterized by helical spin textures and Majorana fermions[69].

Topological insulators come in 2D and 3D varieties, with the 2D topological insulators, known also as quantum spin Hall insulators

(Fig. 3a), originally predicted for graphene[70] and HgTe/CdTe quantum wells[71], and first discovered in the latter[72] (Fig. 3b). They were also reported in InAs/GaSb quantum wells[73]. These compounds are composed of heavy elements and therefore exhibit strong bulk SO interactions. In the quantum spin Hall insulator, the bulk is insulating and two 1D conduction channels exist on each edge. On one edge, two channels are counter-propagating while carrying opposite spin, thus forming a helical spin pair (Fig. 3a). In quantum spin Hall insulators the top of the uppermost valence sub-band — split from the other sub-bands by the SO interaction — is above the bottom of the lowest sub-band in the conduction band. In this inverted band structure, a gap opens due to interaction between the valence and conduction sub-bands, and the SO interaction ensures an odd number of helical pairs on each edge of the system. As opposed to the quantum Hall insulator, the quantum spin Hall insulator exists at zero magnetic field and the robustness of the edge modes is protected by time-reversal symmetry — a property preserved by the SO interaction. Backscattering of the quantum spin Hall edge is strongly suppressed because scattering into a state of opposite momentum requires jumping to the opposite edge if spin orientation is preserved. Magnetic scattering is among the factors that limit the coherence of quantum spin Hall edge states. In today's experiments, these edge states are observed on the micrometre scale, as opposed to the millimetre scale for quantum Hall edge states.

Three-dimensional topological insulators are a dimensional extension of the 2D concept. Again, heavy element compounds such as Bi_2Se_3, Bi_xSb_{1-x} and Bi_2Te_3, which all have strong bulk SO interactions, exhibit the topological insulator phase[69]. Instead of merely exhibiting 1D channels, the edges carry a surface state that is characterized by a Rashba spin texture. Namely, spin is
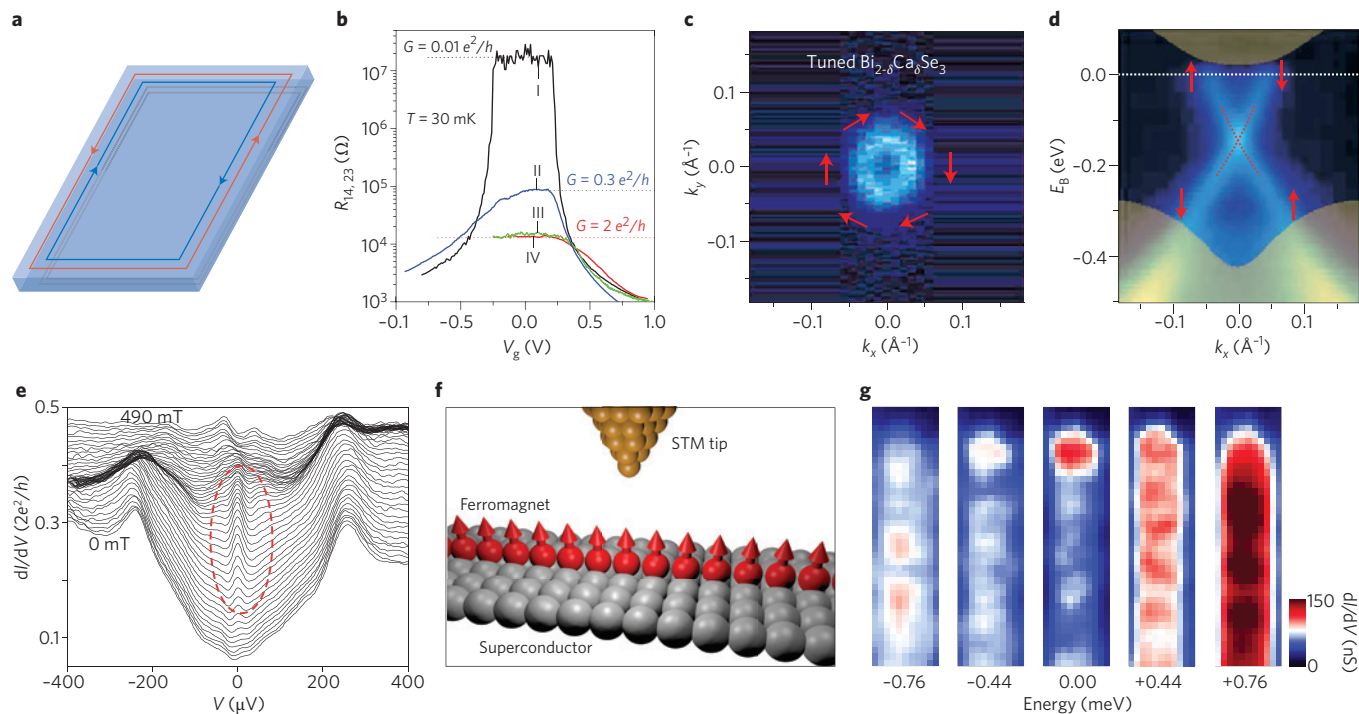
Figure 3 | Topological insulators. a, Schematic of the quantum spin Hall insulator, which is insulating in the bulk and supports pure spin current flow at its edges. The counter-propagating currents (red and blue lines) carry opposite spin polarization. **b**, Experimental evidence of the quantum spin Hall effect in HgTe quantum wells[72]: the longitudinal resistance of the device is represented as a function of the gate voltage V_g. When the Fermi level is tuned at the compensation point, the device shows a quantized conductance G corresponding to the quantum spin Hall effect. Note that sample I (black curve) is a normal quantum well, while samples II–IV correspond to inverted quantum wells of various areas. (Curves III and IV possess the same G.) **c,d**, 2D mapping of the Fermi surface (**c**) and band structure (**d**) of a 3D topological insulator, measured by ARPES[74]. The red arrows represent spin direction. **e**, Magnetic field-dependent spectroscopy of a 1D topological superconductor made of an InSb nanowire, exhibiting a zero-bias peak at finite magnetic field[81] (red oval). **f,g**, Scanning tunnelling microscopy (STM) set-up (**f**) and conductance maps (**g**) demonstrating the emergence of zero-bias states at the ends of the chain of the ferromagnetic–superconductor hybrid structure[82] (red dot in the middle panel of **g**). Figure reproduced with permission from: **b**, ref. 72, AAAS; **c,d**, ref. 74, Nature Publishing Group; **e**, ref. 81, AAAS; **f,g**, ref. 82, AAAS.

locked to momentum and always points perpendicular to it (equation 3 in Box 1). This spin texture was directly observed in angle-resolved photoemission spectroscopy (ARPES) experiments[74] (Fig. 3c,d). Spin–momentum locking also suppresses backscattering, which has been reported in scanning tunnelling microscopy experiments[75].

Topological superconductivity can be understood by a simple formula: topological insulator plus superconductivity[76]. Topological superconductivity can be intrinsic to a compound or induced by proximity to a non-topological superconductor. Topological superconductors are characterized by an inverted superconducting gap, although it is not yet clear how to detect the sign of the gap experimentally. The most remarkable manifestations of topological superconductivity are related to its edge states and derive from the properties of the edge states of a topological insulator. Superconductivity transforms electrons in the edge states into Bogoliubov quasiparticles; that is, coherent superpositions of electrons and holes that necessarily possess particle–hole symmetry. Namely, if there is a state at positive energy there must be a state at negative energy of the same magnitude, with zero energy being the Fermi level. If there is an odd number of states, particle–hole symmetry dictates that one of the states must be pinned to zero energy. This is the case in topological superconductors due to the odd number of helical pairs on each edge of the system. The zero state or mode is then known as a Majorana fermion, because it corresponds to its own antiparticle[76]. Realizing Majorana fermions by combining 2D or 3D topological insulators with conventional superconductors is an active research area[77].

Initial experimental evidence of Majorana fermions was obtained in 1D systems; that is, not from 2D or 3D topological insulating phases. Nevertheless, the SO interaction has been the key ingredient in this case as well. A 1D wire of InSb — a semiconductor with strong Rashba SO interaction — has an electronic spectrum that consists of two spin-resolved parabolas shifted in opposite directions in momentum space (Fig. 2a). Applying an external magnetic field perpendicular to the intrinsic Rashba field mixes the two sub-bands and opens a gap at the crossing point. If the Fermi level is inside this gap, we obtain a helical liquid situation similar to a single edge of a quantum spin Hall insulator: spin-up electrons are only allowed to travel to the right, whereas spin-down electrons only travel to the left[78]. Coupling a conventional s-wave superconductor by proximity to the semiconductor nanowire adds particle–hole symmetry and produces Majorana fermion bound states at the ends of the nanowire[79,80]. Majorana fermions should manifest themselves as peaks in conductance at zero bias, which were indeed observed in a tunnelling experiment (Fig. 3e). Interestingly, when the external magnetic field is aligned with the internal Rashba field, no sub-band hybridization occurs and the gap at zero momentum does not open. In this case Majorana fermions are not expected and the zero-bias peak vanishes[81].

Another recent experiment has attempted to look for Majorana fermions in chains of magnetic atoms on a superconductor surface[82]. The ingredients of this approach are essentially the same as with semiconductor nanowires, but with several remarkable differences. First, the SO interaction in this case is proposed to originate

Box 3 | The concept of pseudospin.

Pseudospin in materials. Although spin is the quantized intrinsic angular momentum of a particle, many other physical quantities can act as an effective spin-1/2, which is referred to as pseudospin. This concept was originally introduced by Heisenberg to describe the structure of the atomic nucleus as composed of neutrons and protons, which he modelled as two states of the same particle[147]. In this context, a pseudospin is a coherent superposition of two quantum states and is described in terms of Pauli matrices for spin-1/2, $\boldsymbol{\sigma} = (\sigma_x, \sigma_y, \sigma_z)$. Although Nambu pseudospin was introduced decades ago to describe quasiparticles in superconductors, recent developments in the physics of SO-coupled transport have identified new degrees of freedom that can be accounted for within the pseudospin language[89]. In hexagonal 2D diamonds, the pseudospin is composed of the sublattices[92], whereas in TMDC it describes the valence and conduction bands of the transition metal[95]. In van der Waals bilayers, when the layer index is a good quantum number, a layer pseudospin can also be identified[148]. Finally, in cold-atom systems, the spin-1/2 pseudospin is defined by two hyperfine split states that can be, for example, coherently coupled by a laser[149].

The concept of pseudospin is useful for predicting and interpreting the transport properties of the various systems mentioned above, in particular when a Rashba-type pseudospin–orbit coupling is present[89]. Nonetheless, it has an important limitation: the nature of the pseudospin (such as sublattice or layer index) is a material property — not an intrinsic property of the carrier, like the spin degree of freedom (except in the case of cold atoms). Therefore, it may not be continuous at the interfaces between different materials[148].

Pseudospin–orbit coupling in cold atoms. To exemplify the use of the pseudospin concept, let us consider a simple example of cold atoms. We imagine that two atomic hyperfine states ($\Psi_\uparrow$ and $\Psi_\downarrow$, selected from a large integer-spin hyperfine multiplet), representing the two states of the pseudospin, are coupled by Raman lasers. The single-particle Hamiltonian is then given by

$$\hat{H} = -\frac{\hbar^2}{2m}\left(\frac{\partial^2}{\partial x^2}+\frac{\partial^2}{\partial y^2}\right)\begin{pmatrix}1 & 0\\0 & 1\end{pmatrix} - \frac{\Delta}{2}\begin{pmatrix}1 & 0\\0 & -1\end{pmatrix} - \frac{\Omega}{2}\begin{pmatrix}0 & e^{ik_p x}\\e^{-ik_p x} & 0\end{pmatrix} \quad (4)$$

where Ω is determined by the strength of the lasers (chosen to point along the x direction) and k_p is the photon wavevector. The Zeeman splitting Δ is controlled by the external magnetic field, and m is the mass of the atoms. We have ignored motion in the z direction, which is justifiable as long as the confining potential is tight in this direction.

The Schrödinger equation for the atoms, $\hat{H}\Psi = E\Psi$, with $\Psi = (\Psi_\uparrow(x, y), \Psi_\downarrow(x, y))$, is now rotated according to $\Psi = Q\phi$. Here Q is the 2 × 2 matrix that diagonalizes the spin part of the Hamiltonian such that

$$Q^{-1}\left(-\frac{\Delta}{2}\begin{pmatrix}1 & 0\\0 & -1\end{pmatrix} - \frac{\Omega}{2}\begin{pmatrix}0 & e^{ik_p x}\\e^{-ik_p x} & 0\end{pmatrix}\right)Q = -\frac{1}{2}\sqrt{\Omega^2 + \Delta^2}$$

The kinetic-energy part of the Schrödinger equation transforms according to

$$-\frac{\hbar^2}{2m}Q^{-1}\left(\frac{\partial^2}{\partial x^2}+\frac{\partial^2}{\partial y^2}\right)\begin{pmatrix}1 & 0\\0 & 1\end{pmatrix}(Q\phi)$$

The laser field gives $Q = Q(x, y)$, which leads to terms that are linear in momentum in the Schrödinger equation for ϕ. One of these terms is a pseudo-SO coupling $\gamma\sigma_x(\partial/\partial x) \propto \gamma\sigma_x p_x$, with $\gamma = \hbar k_p \Omega/2m\sqrt{(\Omega^2 + \Delta^2)}$. The Rashba pseudo-SO coupling can be engineered by employing more involved laser-coupling schemes[150].

---

from the superconductor (Pb used in the experiment has a strong intrinsic SO interaction). Second, time-reversal symmetry is broken by the magnetization of the chain rather than by an external field. Experimentally, zero-bias states were detected by a scanning tunnelling microscopy experiment at the ends of the atomic chains (Fig. 3f,g). A similar outcome would have been possible if the magnetic atoms spontaneously formed a spin helix, thereby creating a synthetic SO interaction along the chain, like in the case of cold atoms discussed below[83].

The significance of this research direction goes beyond the discovery of new topological classes of matter. In the case of helical edge states, the absence of backscattering at zero magnetic field may in the future play a role in reducing dissipation in spintronic and electronic circuits. Majorana bound states are expected to exhibit non-Abelian exchange statistics[84]. This means that, as opposed to conventional fermions and bosons, when one Majorana bound state is moved around another following a closed loop, the system undergoes a transition to a new ground state of distinctly different charge. This non-Abelian property is yet to be demonstrated experimentally. If achieved, it may open the door to the realization of topological quantum computing, in which error-protected quantum operations are performed by moving Majorana fermions around each other (also known as braiding[85]).

Topological states that do not involve SO coupling have been proposed theoretically[86,87]. Such states rely on other crystalline symmetries that play the role of the SO interaction. However, the SO interaction has clearly been essential for uncovering the first wave of experiments and concepts in the field of topological condensed-matter systems.

Low-dimensional Dirac systems

Honeycomb crystals are another class of materials in which topological phases have been identified. In these systems, which present striking similarities with 2D relativistic massive particles, the pseudospin degree of freedom (see below) couples linearly to the electron's momentum to create a pseudo-Dirac kinetic term. The realization of systems that display Dirac-type Hamiltonians dates back to the exploration of superfluidity in ³He (ref. 88) and d-wave superconductivity[89]. In such systems, the momentum of the quasiparticle is directly coupled to its Nambu pseudospin — a spinor formed by its electron and hole parts (Box 3) — thus providing an analogue of the quantum Hall effect in the absence of magnetic fields[90]. More recently, the realization of 2D honeycomb crystals displaying a Dirac cone at the high-symmetry K and K′ points has introduced a new paradigm for effective relativistic condensed-matter physics (Fig. 4a,b).

The physics of Dirac particles introduces a wealth of thought-provoking phenomena, among which Klein tunnelling and zitterbewegung are probably the most illustrative. Klein tunnelling is the absence of backscattering from a potential (such as defects and impurities) due to the penetration of negative-energy particles into the barrier, which results in large mobilities[91] in the context of topological insulators, as mentioned above. Zitterbewegung is the jittering or trembling motion of the carrier, which is a direct consequence of locking between the momentum **p** and the (pseudo)spin momentum. From the perspective of Dirac physics, this effect stems from time-dependent interferences between positive- and negative-energy particles (positrons and electrons, respectively).
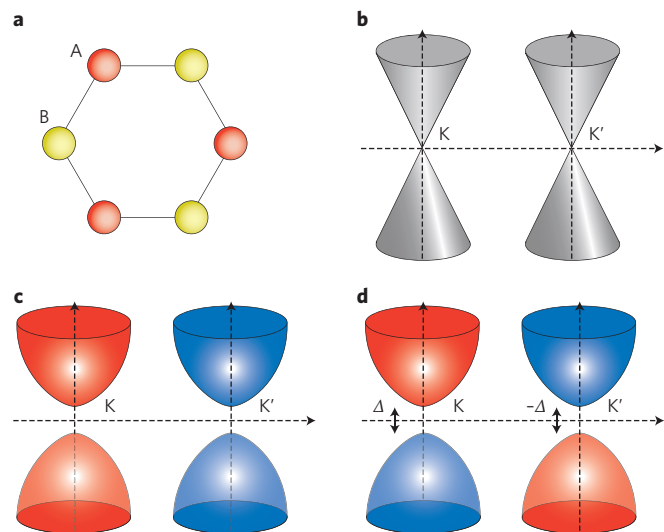
Figure 4 | Low-dimensional Dirac materials. a, Schematic of the hexagonal honeycomb crystal. Sites A and B constitute the pseudospin states. **b**, Low-energy band structure of graphene, comprising two Dirac cones located at the K and K′ points of the Brillouin zone. The chirality of the bands is opposite at these two points. **c**, Low-energy band structure of a transition metal dichalcogenide monolayer. The inversion asymmetry induces a gap and SO coupling induces a supplementary spin splitting. **d**, Low-energy band structure of Haldane's model[98]: the gap is $+\Delta$ at K and $-\Delta$ at K′, thus enabling the emergence of the quantum anomalous Hall effect (that is, a net flow of charge). In **c**,**d**, red and blue correspond to majority and minority spin projections, respectively.

Although the existence of Dirac cones in graphene was realized around 60 years ago[92], it has only reached its full potential recently thanks to the rise of experimental graphene[93]. In this system, the pseudospin corresponds to the two lattice sites composing the motif of the hexagonal lattice. Formally, the (pseudo) SO coupling does not arise from structural inversion asymmetry and hence cannot formally be referred to as Rashba SO coupling. In fact, one of the virtues of the development of graphene has been to shed light on a variety of novel solid-state materials that display a Dirac cone at low energy (Box 3). These materials include 2D graphene-like crystals such as silicene, germanene, stanene and hexagonal boron nitride (hBN), and transition metal-based dichalcogenides (TMDCs) such as MoS_2 and WSe_2 (ref. 94). They all display an orbital gap at their high symmetry K and K′ points, where the linear momentum and pseudospin degrees of freedom are locked. The pseudospin can be a superposition of lattice sites (2D diamonds) or a superposition of unperturbed orbitals (TMDCs). Because these materials possess very flexible properties, they present a unique playground for exploring the Dirac world at the solid-state level.

Analogous to the topological insulators presented in the previous section, honeycomb crystals also display a quantum Hall effect in the insulating regime. The subtlety is that because, in this case, the number of Dirac cones is even, the nature of the quantum Hall effect depends on the origin of the gap. For instance, if the symmetry between the two sublattices is broken (as in the case of TMDCs or hBN; Fig. 4c), the two valleys contribute to an opposite quantum Hall conductivity, thus resulting in a quantum valley Hall effect[95] (charge-neutral current, similar to the quantum spin Hall effect). Similarly, the gap induced by SO coupling results in a quantum spin Hall effect but a vanishing quantum valley Hall effect[70] (as in silicene or germanene). Interestingly, the quantum spin Hall effect is accompanied by spin-polarized edge currents similar to those observed in topological insulators[72,96]. Finally, a last interesting situation is obtained when coupling the honeycomb crystal to an antiferromagnetic insulator[97] (that is, both spatial and time-reversal symmetries are broken), thereby realizing the original Haldane model[98] (Fig. 4d). In this case, the contributions of the two valleys to the quantum Hall effect no longer compensate for each other, thus resulting in a quantum anomalous Hall effect — a quantized transverse charge current.

The observation of quantum spin, valley or anomalous Hall effects in low-dimensional Dirac systems (that is, not topological insulators) is still very challenging: to the best of our knowledge, no topological quantum Hall effect at zero magnetic field has been reported for these materials. Nevertheless, the observation of a large spin Hall effect ($\theta_H \approx 20\%$) in graphene (attributed to extrinsic SO coupling[99]), and also the realization of a magnetic-field-induced quantum spin Hall effect, constitute promising progress towards SO-coupled transport[100]. The existence of large intrinsic Rashba SO coupling in silicene, germanene and possibly stanene[94], as well as the recent demonstration of large extrinsic Rashba SO coupling in graphene[101] (~100 meV) could be the foundation for a breakthrough in this field, as Rashba SO coupling enables the coupling between the pseudospin, spin and momentum degrees of freedom.

Efforts have also been applied towards the manipulation of valley polarization and the realization of the valley Hall effect — the generation of a transverse charge-neutral current induced by the Berry curvature — which could be used as a new functional degree of freedom[102,103]. Breaking spatial inversion symmetry by hybridizing graphene with a hBN substrate[104] has enabled the observation of charge-neutral current in graphene[105,106], which may be associated with the spin or valley Hall effect.

The case of TMDCs is worth special attention[107]. Their large band-gap (~1.5–2 eV) enables optical control of the valley population using resonant light[95], as demonstrated experimentally[108,109]. Furthermore, due to their strong SO coupling, valley and spin are coupled (this is particularly true in WSe_2, for instance). The light-induced valley polarization can be used to generate the valley Hall effect[110] or the spin–valley-coupled photogalvanic effect[111]. Inversely, electrically driven emission of circularly polarized light has been demonstrated recently in a p–n junction geometry in a WSe_2 monolayer[112]. The influence of symmetry breaking in TMDC bilayers is also currently attracting much attention. The gap at K and K′ valleys can be modified by applying an inversion-symmetry-breaking perpendicular electric field, as optically probed in bilayer MoS_2 (ref. 113).

Rashba physics with cold-atom systems

Cold-atom systems are an emerging direction for exploring the physics of SO interactions. These are ultracold (0.1–10 µK) clouds of ~10^9 neutral alkali atoms that are trapped in a magnetic or optical confining potential, using the Zeeman or a.c. Stark effect, respectively. This method of trapping essentially isolates the atoms from their environment and thus does not allow them to experience disorder or lattice vibrations. The atoms — either fermions or bosons — interact via short-range interactions, as opposed to the long-ranged Coulomb interactions felt by electrons in solids. The various properties of cold-atom systems, such as confining potential, temperature, density and interaction strength, can be tuned experimentally. The scientific breakthroughs achieved using cold-atom systems are largely attributable to this tunability, and also to the fact that these systems explore new physical regimes beyond those of electrons in solid-state materials or other condensed-matter systems.

For a gas of alkali-metal atoms, the role of spin is played by the atoms' hyperfine spin degrees of freedom (Box 3). Spin–orbit coupling here refers to the coupling between the motion of each neutral atom and its hyperfine spin — not the coupling between the orbital momentum of each atom's valence electron and its spin. Because the atoms are neutral, this SO coupling arises in a different manner than for electrons, and because it must be engineered, it is referred to as synthetic SO coupling (Box 3).
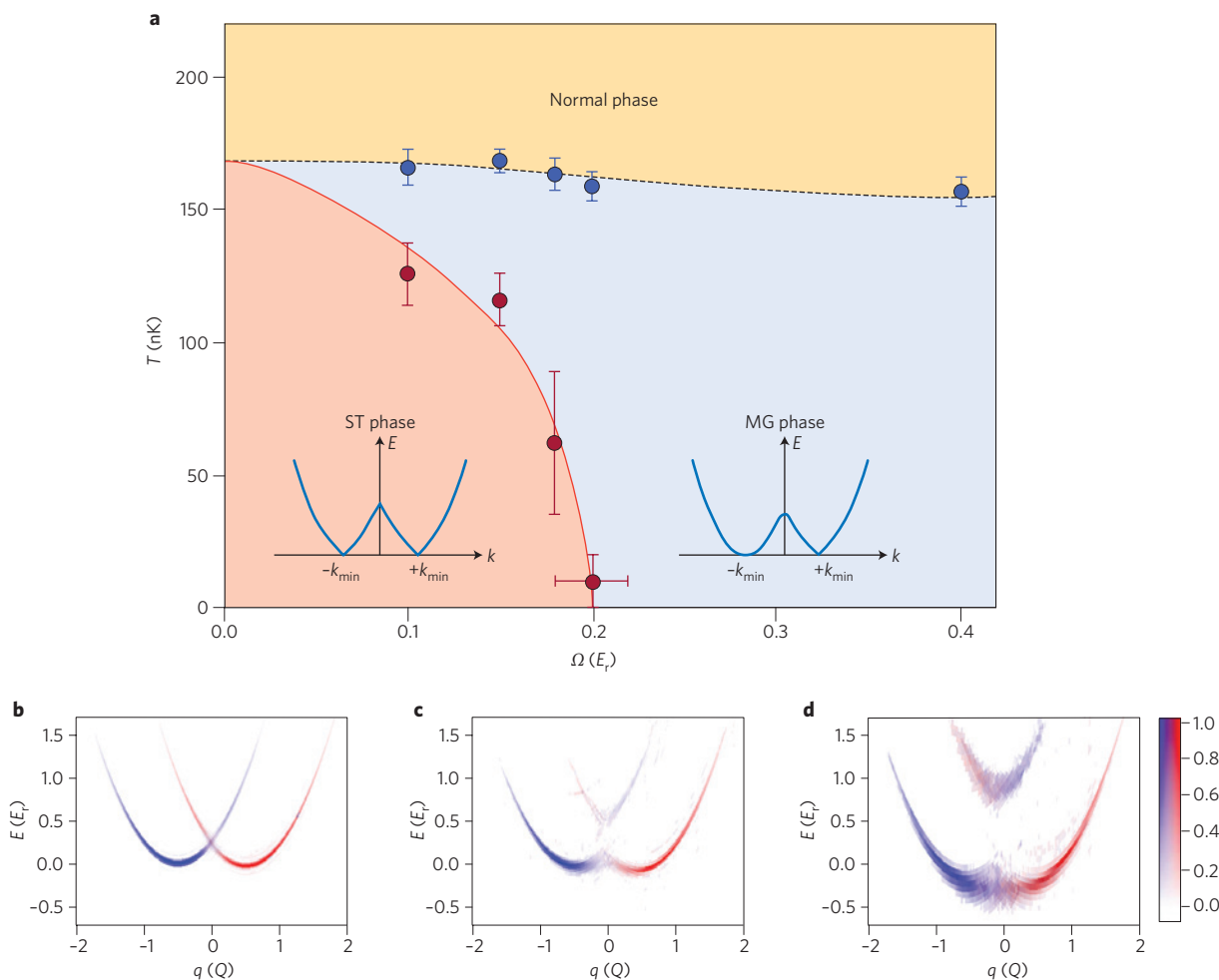
Figure 5 | Tuning spin–orbit coupling in cold-atom gases. a, Finite-temperature phase diagram of a SO-coupled Bose gas. The lines separate stripe phases (ST), magnetized phases (MG) and a normal phase. The horizontal axis corresponds to the strength of the laser (in units of the recoil energy E_r), which determines the strength of the SO coupling[118]. **b–d**, SO-coupled dispersion and SO gap in a gas of fermionic atoms determined by spin-injection spectroscopy. Here, **b**, **c** and **d** are obtained for no, moderate, and strong synthetic SO coupling, respectively. In these measurements, a radiofrequency pulse transfers atoms from the SO-coupled states to an unoccupied hyperfine state. Measuring the number of atoms in this initially unoccupied state as a function of pulse energy gives information on the energy dispersion of the trapped atoms (or, more generally, their spectral function, similar to ARPES in electronic systems). Here, the energies are in units of the recoil energy of the laser that engineers the synthetic SO coupling, and the momentum q is in units of the photon momentum Q (k_p in equation 4 in Box 3)[120]. The colour scale bar indicates the majority (red) and the minority (blue) spin projections. Figure reproduced with permission from: **a**, ref. 118, Nature Publishing Group; **b–d**, ref. 120, APS.

Recent experimental efforts have succeeded in creating this synthetic SO coupling. The first experiment involving bosons saw a transition between phase-mixed and phase-separated dressed spin states in the Bose–Einstein condensate regime[114]. Subsequent experiments on coupling the linear motion of bosonic atoms to their hyperfine spin have demonstrated strong synthetic orbital magnetic fields[115], changes in the dipole collective mode due to SO coupling[116], Zitterbewegung[117], and, very recently, a map of the finite-temperature phase diagram[118] (Fig. 5a). Similar efforts with fermionic atoms[119] demonstrated the emergence of a SO gap in these systems[120] (Fig. 5b–d), as well as realization of the Haldane model[121].

Ongoing and future efforts are dedicated to engineering more sophisticated synthetic SO coupling schemes. This paves the way for a variety of fundamental research. First, by serving as controlled quantum simulators for electrons, fermionic systems may allow for the singling out of particular effects, such as the competition between SO coupling and many-body interactions. Second, SO coupling in cold-atom systems gives rise to new phenomena arising from coupling between hyperfine spin and linear motion. One example of this is the observation of synthetic partial waves in interatomic

collisions[122]. Finally, both fermionic and bosonic systems enable completely novel states of matter to be engineered that have no analogue in the solid state. Examples of these are SO-coupled Mott insulators and superfluids that arise in systems of strongly interacting SO-coupled cold atoms in optical lattices[123–126]. Most spectacular, perhaps, is the outlook of SO-coupled cold atoms to realize a host of exotic phases, known as bosonic topological insulators[127,128]. These phases are reminiscent of electronic topological insulators in that they support edge states, but, contrary to electronic topological states, arise only in the presence of interactions.

Summary and outlook

The advancement of research in the SO-coupled transport of inversion asymmetric systems has been extremely creative over the past 10 years. Wide areas of physics and materials science such as metallic spintronics, van der Waals materials and cold-atom systems — traditionally treated on entirely different footings — are now converging under the umbrella of spin–orbitronics. Traditional spintronics has already been through two major revolutions in its history (giant magnetoresistance and spin-transfer torques) and is

currently experiencing its third thanks to the development of chiral magnetic structures. On the low-dimensional side, although it is not entirely clear whether graphene will eventually keep its promises, novel systems such as TMDC, silicene, germanene, stanene and topological insulators are offering even broader opportunities for materials design. Finally, Rashba-like SO coupling enables unique topological properties that are, for example, expected in superconductors and cold-atom systems. Exotic states of matter such as bosonic topological states stabilized by interactions will surely keep the heat on for several decades.

We chose to focus this Review on a select number of topics whose development is particularly promising, yet there are a number of additional subjects that deserve attention but could not be included in this brief overview. The electrical and optical control of spin in semiconductors is a vast area for which we could only give an imperfect account[129]. For instance, electron dipole spin resonance could have been the subject of a much deeper presentation. We also wish to mention that novel materials displaying extremely large Rashba-type SO coupling in their bulk are currently receiving significant interest (such as BiTeI polar semiconductors or $R_2Ir_2O_7$ pyrochlores[130], where R is a rare earth element), which are paving the way towards experimental realization of Weyl semimetals[131,132] and other exotic phases[133]. Finally, concepts related to Rashba SO coupling in electronic systems have also been recently extended to the optical properties of chiral biological systems[134].

References

1. Dresselhaus, G. Spin-orbit coupling effects in zinc blende structures. *Phys. Rev.* **100**, 580–586 (1955).
2. Rashba, E. Properties of semiconductors with an extremum loop. 1. Cyclotron and combinational resonance in a magnetic field perpendicular to the plane of the loop. *Sov. Phys. Solid State* **2**, 1109–1122 (1960).
3. Vas'ko, F. T. Spin splitting in the spectrum of two-dimensional electrons due to the surface potential. *P. Zh. Eksp. Teor. Fiz.* **30**, 574–577 (1979).
4. Bychkov, Y. A. & Rashba, E. I. Properties of a 2D electron gas with lifted spectral degeneracy. *P. Zh. Eksp. Teor. Fiz.* **39**, 66–69 (1984).
5. Fabian, J., Matos-Abiague, A., Ertler, C., Stano, P. & Zutic, I. Semiconductor spintronics. *Acta Phys. Slovaca* **57**, 565–907 (2007).
6. Chappert, C., Fert, A. & Van Dau, F. N. The emergence of spin electronics in data storage. *Nature Mater.* **6**, 813–823 (2007).
7. Jungwirth, T., Wunderlich, J. & Olejník, K. Spin Hall effect devices. *Nature Mater.* **11**, 382–390 (2012).
8. Dyakonov, M. I. & Perel, V. I. Possibility of orienting electron spins with current. *ZhETF Pis. Red.* **13**, 657–660 (1971).
9. Hirsch, J. Spin Hall effect. *Phys. Rev. Lett.* **83**, 1834–1837 (1999).
10. Murakami, S., Nagaosa, N. & Zhang, S.-C. Dissipationless quantum spin current at room temperature. *Science* **301**, 1348–1351 (2003).
11. Sinova, J. *et al.* Universal intrinsic spin Hall effect. *Phys. Rev. Lett.* **92**, 126603 (2004).
12. Xiao, D., Chang, M.-C. & Niu, Q. Berry phase effects on electronic properties. *Rev. Mod. Phys.* **82**, 1959–2007 (2010).
13. Kato, Y. K., Mährlein, S., Gossard, A. C. & Awschalom, D. D. Observation of the spin Hall effect in semiconductors. *Science* **306**, 1910–1913 (2004).
14. Wunderlich, J., Kaestner, B., Sinova, J. & Jungwirth, T. Experimental observation of the spin-Hall effect in a two dimensional spin-orbit coupled semiconductor system. *Phys. Rev. Lett.* **94**, 047204 (2005).
15. Wunderlich, J. *et al.* Spin Hall effect transistor. *Science* **330**, 1801–1804 (2010).
16. Valenzuela, S. O. & Tinkham, M. Direct electronic measurement of the spin Hall effect. *Nature* **442**, 176–179 (2006).
17. Hoffmann, A. Spin Hall effects in metals. *IEEE Trans. Magn.* **49**, 5172–5193 (2013).
18. Sinova, J., Valenzuela, S. O., Wunderlich, J., Back, C. H. & Jungwirth, T. Spin Hall effects. *Rev. Mod. Phys.* http://journals.aps.org/rmp/accepted/58077E11 Q8f15e01e0aa5510b2767e3da25148b87 (2015).
19. Rauch, H. *et al.* Verification of coherent spinor rotation of fermions. *Phys. Lett. A* **54**, 425–427 (1975).
20. König, M. *et al.* Direct observation of the Aharonov–Casher Phase. *Phys. Rev. Lett.* **96**, 076804 (2006).
21. Bergsten, T., Kobayashi, T., Sekine, Y. & Nitta, J. Experimental demonstration of the time reversal Aharonov–Casher effect. *Phys. Rev. Lett.* **97**, 196803 (2006).
22. Aharonov, Y. & Casher, A. Topological quantum effects for neutral particles. *Phys. Rev. Lett.* **53**, 319–321 (1984).
23. Nitta, J., Akazaki, T., Takayanagi, H. & Enoki, T. Gate control of spin-orbit interaction in an inverted InGaAs/InAlAs heterostructure. *Phys. Rev. Lett.* **78**, 1335–1338 (1997).
24. Wunderlich, J. *et al.* Spin-injection Hall effect in a planar photovoltaic cell. *Nature Phys.* **5**, 675–681 (2009).
25. Ivchenko, E. L. & Pikus, G. E. New photogalvanic effect in gyrotropic crystals. *JETP Lett.* **27**, 604–608 (1978).
26. Ganichev, S. D. Spin-galvanic effect and spin orientation by current in non-magnetic semiconductors. *Int. J. Mod. Phys. B* **22**, 1–26 (2008).
27. Rojas-Sánchez, J. C. *et al.* Spin-to-charge conversion using Rashba coupling at the interface between non-magnetic materials. *Nature Commun.* **4**, 2944 (2013).
28. Edelstein, V. M. Spin polarization of conduction electrons induced by electric current in two-dimensional asymmetric electron systems. *Solid State Commun.* **73**, 233–235 (1990).
29. Kato, Y. K., Myers, R., Gossard, A. & Awschalom, D. D. Current-induced spin polarization in strained semiconductors. *Phys. Rev. Lett.* **93**, 176601 (2004).
30. Ganichev, S. D. *et al.* Electric current-induced spin orientation in quantum well structures. *J. Magn. Magn. Mater.* **300**, 127–131 (2006).
31. Schultz, M. *et al.* Rashba spin splitting in a gated HgTe quantum well. *Semicond. Sci. Technol.* **11**, 1168–1172 (1996).
32. Datta, S. & Das, B. Electronic analog of the electro-optic modulator. *Appl. Phys. Lett.* **56**, 665–667 (1990).
33. Koo, H. C. *et al.* Control of spin precession in a spin-injected field effect transistor. *Science* **325**, 1515–1518 (2009).
34. Ohe, J., Yamamoto, M., Ohtsuki, T. & Nitta, J. Mesoscopic Stern–Gerlach spin filter by nonuniform spin-orbit interaction. *Phys. Rev. B* **72**, 041308 (2005).
35. Kohda, M. *et al.* Spin–orbit induced electronic spin separation in semiconductor nanostructures. *Nature Commun.* **3**, 1082 (2012).
36. Herbert, S. T., Muhammad, M. & Johnson, M. All-electric quantum point contact spin-polarizer. *Nature Nanotech.* **4**, 759–764 (2009).
37. Frolov, S. M. *et al.* Ballistic spin resonance. *Nature* **458**, 868–871 (2009).
38. Nowack, K. C., Koppens, F. H. L., Nazarov, Y. V. & Vandersypen, L. M. K. Coherent control of a single electron spin with electric fields. *Science* **318**, 1430–1433 (2007).
39. Nadj-Perge, S., Frolov, S. M., Bakkers, E. P. A. M. & Kouwenhoven, L. P. Spin-orbit qubit in a semiconductor nanowire. *Nature* **468**, 1084–1087 (2010).
40. Van den Berg, J. *et al.* Fast spin-orbit qubit in an indium antimonide nanowire. *Phys. Rev. Lett.* **110**, 066806 (2013).
41. Petersson, K. D. *et al.* Circuit quantum electrodynamics with a spin qubit. *Nature* **490**, 380–383 (2012).
42. Dyakonov, M. & Perel, V. Spin relaxation of conduction electrons in noncentrosymmetric semiconductors. *Sov. Phys. Solid State* **13**, 3023–3026 (1972).
43. Averkiev, N. S. & Golub, L. E. Giant spin relaxation anisotropy in zinc-blende heterostructures. *Phys. Rev. B* **60**, 15582–15584 (1999).
44. Schliemann, J., Egues, J. C. & Loss, D. Nonballistic spin-field-effect transistor. *Phys. Rev. Lett.* **90**, 146801 (2003).
45. Bernevig, B. A., Orenstein, J. & Zhang, S.-C. Exact SU(2) symmetry and persistent spin helix in a spin-orbit coupled system. *Phys. Rev. Lett.* **97**, 236601 (2006).
46. Koralek, J. D. *et al.* Emergence of the persistent spin helix in semiconductor quantum wells. *Nature* **458**, 610–613 (2009).
47. Sasaki, A. *et al.* Direct determination of spin–orbit interaction coefficients and realization of the persistent spin helix symmetry. *Nature Nanotech.* **9**, 703–709 (2014).
48. Slonczewski, J. C. Current-driven excitation of magnetic multilayers. *J. Magn. Magn. Mater.* **159**, L1–L7 (1996).
49. Berger, L. Emission of spin waves by a magnetic multilayer traversed by a current. *Phys. Rev. B* **54**, 9353–9358 (1996).
50. Bernevig, B. A. & Vafek, O. Piezo-magnetoelectric effects in p-doped semiconductors. *Phys. Rev. B* **72**, 033203 (2005).
51. Manchon, A. & Zhang, S. Theory of nonequilibrium intrinsic spin torque in a single nanomagnet. *Phys. Rev. B* **78**, 212405 (2008).
52. Miron, I. M. *et al.* Perpendicular switching of a single ferromagnetic layer induced by in-plane current injection. *Nature* **476**, 189–193 (2011).
53. Chernyshov, A. *et al.* Evidence for reversible control of magnetization in a ferromagnetic material by means of spin–orbit magnetic field. *Nature Phys.* **5**, 656–659 (2009).
54. Miron, I. M. *et al.* Current-driven spin torque induced by the Rashba effect in a ferromagnetic metal layer. *Nature Mater.* **9**, 230–234 (2010).
55. Kurebayashi, H. *et al.* An antidamping spin–orbit torque originating from the Berry curvature. *Nature Nanotech.* **9**, 211–217 (2014).

56. Garello, K. *et al.* Symmetry and magnitude of spin–orbit torques in ferromagnetic heterostructures. *Nature Nanotech.* **8,** 587–593 (2013).
57. Liu, L. *et al.* Spin-torque switching with the giant spin Hall effect of tantalum. *Science* **336,** 555–558 (2012).
58. Mellnik, A. R. *et al.* Spin-transfer torque generated by a topological insulator. *Nature* **511,** 449–451 (2014).
59. Fan, Y. *et al.* Magnetization switching through giant spin–orbit torque in a magnetically doped topological insulator heterostructure. *Nature Mater.* **13,** 699–704 (2014).
60. Železný, J. *et al.* Relativistic Néel-order fields induced by electrical current in antiferromagnets. *Phys. Rev. Lett.* **113,** 157201 (2014).
61. Wadley, P. *et al.* Electrical switching of an antiferromagnet. Preprint at http://arxiv.org/abs/1503.03765 (2015).
62. Dzyaloshinskii, I. E. Thermodynamic theory of weak ferromagnetism in antiferromagnetic substances. *Sov. Phys. JETP* **5,** 1259–1262 (1957).
63. Moriya, T. Anisotropic superexchange interaction and weak ferromagnetism. *Phys. Rev.* **120,** 91–98 (1960).
64. Nagaosa, N. & Tokura, Y. Topological properties and dynamics of magnetic skyrmions. *Nature Nanotech.* **8,** 899–911 (2013).
65. Zakeri, K. *et al.* Asymmetric spin-wave dispersion on Fe(110): Direct evidence of the Dzyaloshinskii–Moriya interaction. *Phys. Rev. Lett.* **104,** 137203 (2010).
66. Onose, Y. *et al.* Observation of the magnon Hall effect. *Science* **329,** 297–299 (2010).
67. Matsumoto, R. & Murakami, S. Theoretical prediction of a rotating magnon wave packet in ferromagnets. *Phys. Rev. Lett.* **106,** 197202 (2011).
68. Manchon, A., Ndiaye, P. B., Moon, J., Lee, H. & Lee, K. Magnon-mediated Dzyaloshinskii–Moriya torque in homogeneous ferromagnets. *Phys. Rev. B* **90,** 224403 (2014).
69. Hasan, M. Z. & Kane, C. L. Colloquium: Topological insulators. *Rev. Mod. Phys.* **82,** 3045–3067 (2010).
70. Kane, C. L. & Mele, E. J. Quantum spin Hall effect in graphene. *Phys. Rev. Lett.* **95,** 226801 (2005).
71. Bernevig, B. A., Hughes, T. L. & Zhang, S.-C. Quantum spin Hall effect and topological phase transition in HgTe quantum wells. *Science* **314,** 1757–1761 (2006).
72. König, M. *et al.* Quantum spin Hall insulator state in HgTe quantum wells. *Science* **318,** 766–770 (2007).
73. Knez, I., Du, R.-R. & Sullivan, G. Evidence for helical edge modes in inverted InAs/GaSb quantum wells. *Phys. Rev. Lett.* **107,** 136603 (2011).
74. Hsieh, D. *et al.* A tunable topological insulator in the spin helical Dirac transport regime. *Nature* **460,** 1101–1105 (2009).
75. Roushan, P. *et al.* Topological surface states protected from backscattering by chiral spin texture. *Nature* **460,** 1106–1109 (2009).
76. Beenakker, C. W. J. Search for Majorana fermions in superconductors. *Annu. Rev. Condens. Matter Phys.* **4,** 113–136 (2013).
77. Fu, L. & Kane, C. Superconducting proximity effect and Majorana fermions at the surface of a topological insulator. *Phys. Rev. Lett.* **100,** 096407 (2008).
78. Středa, P. & Šeba, P. Antisymmetric spin filtering in one-dimensional electron systems with uniform spin-orbit coupling. *Phys. Rev. Lett.* **90,** 256601 (2003).
79. Lutchyn, R., Sau, J. & Das Sarma, S. Majorana fermions and a topological phase transition in semiconductor-superconductor heterostructures. *Phys. Rev. Lett.* **105,** 077001 (2010).
80. Oreg, Y., Refael, G. & von Oppen, F. Helical liquids and Majorana bound states in quantum wires. *Phys. Rev. Lett.* **105,** 177002 (2010).
81. Mourik, V. *et al.* Signatures of Majorana fermions in hybrid superconductor-semiconductor nanowire devices. *Science* **336,** 1003–1007 (2012).
82. Nadj-Perge, S. *et al.* Observation of Majorana fermions in ferromagnetic atomic chains on a superconductor. *Science* **346,** 602–607 (2014).
83. Choy, T.-P., Edge, J. M., Akhmerov, A. R. & Beenakker, C. W. J. Majorana fermions emerging from magnetic nanoparticles on a superconductor without spin-orbit coupling. *Phys. Rev. B* **84,** 195442 (2011).
84. Moore, G. & Read, N. Nonabelions in the fractional quantum Hall effect. *Nucl. Phys. B* **360,** 362–396 (1991).
85. Nayak, C., Simon, S., Stern, A., Freedman, M. & Das Sarma, S. Non-Abelian anyons and topological quantum computation. *Rev. Mod. Phys.* **80,** 1083–1159 (2008).
86. Fu, L. Topological crystalline insulators. *Phys. Rev. Lett.* **106,** 106802 (2011).
87. Alexandradinata, A., Fang, C., Gilbert, M. J. & Bernevig, B. A. Spin-orbit-free topological insulators without time-reversal symmetry. *Phys. Rev. Lett.* **113,** 116403 (2014).
88. Ikegami, H., Tsutsumi, Y. & Kono, K. Chiral symmetry breaking in ³He-A. *Science* **341,** 59–62 (2013).
89. Wehling, T. O., Black-Schaffer, A. M. & Balatsky, A. V. Dirac materials. *Adv. Phys.* **63,** 1–76 (2014).
90. Volovik, G. E. An analog of the quantum Hall effect in a superfluid ³He film. *Sov. Phys. JETP* **67,** 1804–1811 (1988).
91. Katsnelson, M. I., Novoselov, K. S. & Geim, A. K. Chiral tunnelling and the Klein paradox in graphene. *Nature Phys.* **2,** 620–625 (2006).
92. Slonczewski, J. C. & Weiss, P. R. Band structure of graphite. *Phys. Rev.* **109,** 272–279 (1958).
93. Zhang, Y., Tan, Y.-W., Stormer, H. L. & Kim, P. Experimental observation of the quantum Hall effect and Berry's phase in graphene. *Nature* **438,** 201–204 (2005).
94. Han, W., Kawakami, R. K., Gmitra, M. & Fabian, J. Graphene spintronics. *Nature Nanotech.* **9,** 794–807 (2014).
95. Xiao, D., Liu, G.-B., Feng, W., Xu, X. & Yao, W. Coupled spin and valley physics in monolayers of MoS₂ and other group-VI dichalcogenides. *Phys. Rev. Lett.* **108,** 196802 (2012).
96. Roth, A. *et al.* Nonlocal transport in the quantum spin Hall state. *Science* **325,** 294–297 (2009).
97. Qiao, Z. *et al.* Quantum anomalous Hall effect in graphene proximity coupled to an antiferromagnetic insulator. *Phys. Rev. Lett.* **112,** 116404 (2014).
98. Haldane, F. D. M. Model for a quantum Hall effect without Landau levels: Condensed-matter realization of the 'parity anomaly'. *Phys. Rev. Lett.* **61,** 2015–2018 (1988).
99. Balakrishnan, J. *et al.* Giant spin Hall effect in graphene grown by chemical vapour deposition. *Nature Commun.* **5,** 4748 (2014).
100. Young, A. F. *et al.* Tunable symmetry breaking and helical edge transport in a graphene quantum spin Hall state. *Nature* **505,** 528–532 (2014).
101. Marchenko, D. *et al.* Giant Rashba splitting in graphene due to hybridization with gold. *Nature Commun.* **3,** 1232 (2012).
102. Xiao, D., Yao, W. & Niu, Q. Valley-contrasting physics in graphene: Magnetic moment and topological transport. *Phys. Rev. Lett.* **99,** 236809 (2007).
103. Rycerz, A., Tworzydło, J. & Beenakker, C. W. J. Valley filter and valley valve in graphene. *Nature Phys.* **3,** 172–175 (2007).
104. Hunt, B. *et al.* Massive Dirac fermions and Hofstadter butterfly in a van der Waals heterostructure. *Science* **340,** 1427–1430 (2013).
105. Abanin, D. A. *et al.* Giant nonlocality near the Dirac point in graphene. *Science* **332,** 328–330 (2011).
106. Gorbachev, R. V. *et al.* Detecting topological currents in graphene superlattices. *Science* **346,** 448–451 (2014).
107. Xu, X., Yao, W., Xiao, D. & Heinz, T. F. Spin and pseudospins in layered transition metal dichalcogenides. *Nature Phys.* **10,** 343–350 (2014).
108. Mak, K. F., He, K., Shan, J. & Heinz, T. F. Control of valley polarization in monolayer MoS₂ by optical helicity. *Nature Nanotech.* **7,** 494–498 (2012).
109. Zeng, H., Dai, J., Yao, W., Xiao, D. & Cui, X. Valley polarization in MoS₂ monolayers by optical pumping. *Nature Nanotech.* **7,** 490–493 (2012).
110. Mak, K. F., McGill, K. L., Park, J. & McEuen, P. L. Valleytronics. The valley Hall effect in MoS₂ transistors. *Science* **344,** 1489–1492 (2014).
111. Yuan, H. *et al.* Generation and electric control of spin-valley-coupled circular photogalvanic current in WSe₂. *Nature Nanotech.* **9,** 851–857 (2014).
112. Zhang, Y. J., Oka, T., Suzuki, R., Ye, J. T. & Iwasa, Y. Electrically switchable chiral light-emitting transistor. *Science* **344,** 725–728 (2014).
113. Wu, S. *et al.* Electrical tuning of valley magnetic moment through symmetry control in bilayer MoS₂. *Nature Phys.* **9,** 149–153 (2013).
114. Lin, Y.-J., Jimenez-Garcıa, K. & Spielman, I. B. Spin–orbit-coupled Bose–Einstein condensates. *Nature* **471,** 83–86 (2011).
115. Aidelsburger, M. Experimental realization of strong effective magnetic fields in an optical lattice. *Phys. Rev. Lett.* **107,** 255301 (2011).
116. Zhang, J.-Y. *et al.* Collective dipole oscillations of a spin-orbit coupled Bose–Einstein condensate. *Phys. Rev. Lett.* **109,** 115301 (2012).
117. Qu, C., Hamner, C., Gong, M., Zhang, C. & Engels, P. Observation of zitterbewegung in a spin-orbit-coupled Bose–Einstein condensate. *Phys. Rev. A* **88,** 021604 (2013).
118. Ji, S.-C. *et al.* Experimental determination of the finite-temperature phase diagram of a spin–orbit coupled Bose gas. *Nature Phys.* **10,** 314–320 (2014).
119. Wang, P., Yu, Z., Fu, Z., Miao, J. & Huang, L. Spin-orbit coupled degenerate Fermi gases. *Phys. Rev. Lett.* **109,** 095301 (2012).
120. Cheuk, L. W. *et al.* Spin-injection spectroscopy of a spin-orbit coupled Fermi gas. *Phys. Rev. Lett.* **109,** 095302 (2012).
121. Jotzu, G. *et al.* Experimental realization of the topological Haldane model with ultracold fermions. *Nature* **515,** 237–240 (2014).
122. Williams, R. A. *et al.* Synthetic partial waves in ultracold atomic collisions. *Science* **335,** 314–317 (2011).
123. Cole, W. S., Zhang, S., Paramekanti, A. & Trivedi, N. Bose–Hubbard models with synthetic spin-orbit coupling: Mott insulators, spin textures, and superfluidity. *Phys. Rev. Lett.* **109,** 085302 (2012).
124. Radić, J., Di Ciolo, A., Sun, K. & Galitski, V. Exotic quantum spin models in spin-orbit-coupled Mott insulators. *Phys. Rev. Lett.* **109,** 085303 (2012).
125. Cocks, D. *et al.* Time-reversal-invariant Hofstadter–Hubbard model with ultracold Fermions. *Phys. Rev. Lett.* **109,** 205303 (2012).
126. Cai, Z., Zhou, X. & Wu, C. Magnetic phases of bosons with synthetic spin-orbit coupling in optical lattices. *Phys. Rev. A* **85,** 061605 (2012).

127. Chen, X., Gu, Z.-C., Liu, Z.-X. & Wen, X.-G. Symmetry-protected topological orders in interacting bosonic systems. *Science* **338,** 1604–1606 (2012).
128. Vishwanath, A. & Senthil, T. Physics of three-dimensional bosonic topological insulators: Surface-deconfined criticality and quantized magnetoelectric effect. *Phys. Rev. X* **3,** 011016 (2013).
129. Hanson, R. & Awschalom, D. D. Coherent manipulation of single spins in semiconductors. *Nature* **453,** 1043–1049 (2008).
130. Yang, B.-J. & Nagaosa, N. Emergent topological phenomena in thin films of pyrochlore iridates. *Phys. Rev. Lett.* **112,** 246402 (2014).
131. Liu, Z. K. *et al.* Discovery of a three-dimensional topological Dirac semimetal, Na_3Bi. *Science* **343,** 864–867 (2014).
132. Xu, S. *et al.* Observation of Fermi arc surface states in a topological metal. *Science* **347,** 294–298 (2015).
133. Witczak-Krempa, W., Chen, G., Kim, Y. B. & Balents, L. Correlated quantum phenomena in the strong spin-orbit regime. *Annu. Rev. Condens. Matter Phys.* **5,** 57–82 (2014).
134. Naaman, R. & Waldeck, D. H. Chiral-induced spin selectivity effect. *J. Phys. Chem. Lett.* **3,** 2178–2187 (2012).
135. Ast, C. *et al.* Giant spin splitting through surface alloying. *Phys. Rev. Lett.* **98,** 186807 (2007).
136. Winkler, R. *Spin-Orbit Coupling effects in Two-Dimensional Electron and Hole Systems* (Springer, 2003).
137. Dyakonov, M. I. & Kachorovskii, V. Y. Spin relaxation of two-dimensional electrons in noncentrosymmetric semiconductors. *Sov. Phys. Semicond.* **20,** 110–112 (1986).
138. Bihlmayer, G., Koroteev, Y. M., Echenique, P. M., Chulkov, E. V. & Blügel, S. The Rashba-effect at metallic surfaces. *Surf. Sci.* **600,** 3888–3891 (2006).
139. Park, Y. H. *et al.* Separation of Rashba and Dresselhaus spin-orbit interactions using crystal direction dependent transport measurements. *Appl. Phys. Lett.* **103,** 252407 (2013).
140. Nakamura, H., Koga, T. & Kimura, T. Experimental evidence of cubic Rashba effect in an inversion-symmetric oxide. *Phys. Rev. Lett.* **108,** 206601 (2012).
141. LaShell, S., McDougall, B. & Jensen, E. Spin splitting of an Au(111) surface state band observed with angle resolved photoelectron spectroscopy. *Phys. Rev. Lett.* **77,** 3419–3422 (1996).
142. Varykhalov, A. *et al.* Ir(111) surface state with giant Rashba splitting persists under graphene in air. *Phys. Rev. Lett.* **108,** 066804 (2012).
143. King, P. D. C. *et al.* Large tunable Rashba spin splitting of a two-dimensional electron gas in Bi_2Se_3. *Phys. Rev. Lett.* **107,** 096802 (2011).
144. Ishizaka, K. *et al.* Giant Rashba-type spin splitting in bulk BiTeI. *Nature Mater.* **10,** 521–526 (2011).
145. Moser, J. *et al.* Tunneling anisotropic magnetoresistance and spin-orbit coupling in Fe/GaAs/Au tunnel junctions. *Phys. Rev. Lett.* **99,** 056601 (2007).
146. Park, B. G. *et al.* A spin-valve-like magnetoresistance of an antiferromagnet-based tunnel junction. *Nature Mater.* **10,** 347–351 (2011).
147. Heisenberg, W. *Über den Bau der Atomkerne. I. Z. Phys.* **77,** 1–11 (1932).
148. Pesin, D. A. & MacDonald, A. H. Spintronics and pseudospintronics in graphene and topological insulators. *Nature Mater.* **11,** 409–416 (2012).
149. Liu, X., Borunda, M. F., Liu, X. & Sinova, J. Effect of induced spin-orbit coupling for atoms via laser fields. *Phys. Rev. Lett.* **102,** 046402 (2009).
150. Dalibard, J., Gerbier, F., Juzeliunas, G. & Öhberg, P. Artificial gauge potentials for neutral atoms. *Rev. Mod. Phys.* **83,** 1523–1543 (2011).

Additional information

Reprints and permissions information is available online at www.nature.com/reprints. Correspondence should be addressed to A.M.

Competing financial interests

The authors declare no competing financial interests.